HHS Public Access

Author manuscript

Ann Neurol. Author manuscript; available in PMC 2024 September 01.

Published in final edited form as:

Ann Neurol. 2023 September ; 94(3): 442–456. doi:10.1002/ana.26710.

Regional glymphatic abnormality in behavioral variant frontotemporal dementia

Deming Jiang[1], **Li Liu**[1], **Yu Kong**[1], **Zhongyun Chen**[1], **Pedro Rosa–Neto**[2], **Kewei Chen**[3], **Liankun Ren**[1], **Min Chu**[1,*], **Liyong Wu**[1,*], **Frontotemporal Lobar Degeneration Neuroimaging Initiative**[†]

[1]Department of Neurology, Xuanwu Hospital, Capital Medical University, Changchun Street 45, Beijing, China

[2]Alzheimer's Disease Research Unit, McGill Centre for Studies in Aging, Montreal H4H 1R3, Canada

[3]Banner Alzheimer's Institute, University of Arizona, School of Mathematics and Statistics, Arizona Alzheimer's Consortium, Arizona State University, Tempe, USA

Abstract

Objectives: The glymphatic function has not yet been explored in behavioral variant frontotemporal dementia (bvFTD). The spatial correlation between regional glymphatic function and bvFTD remain unknown.

Method: A total of 74 patients with bvFTD and 67 age- and sex-matched healthy controls (HCs) were selected from discovery dataset and replication dataset. All participant underwent neuropsychological assessment. Glymphatic measures including choroid plexus (CP) volume, diffusion tensor imaging along the perivascular (DTI-ALPS) index, and coupling between blood-oxygen-level-dependent signals and cerebrospinal fluid signals (BOLD-CSF coupling), were compared between the two groups. Regional glymphatic function was evaluated by dividing DTI-ALPS and BOLD-CSF coupling into anterior, middle, and posterior regions. BvFTD-related metabolic pattern was identified using spatial covariance analysis based on ^{18}F-FDG-PET.

Results: Patients with bvFTD showed higher CP volume ($P < 0.001$); anterior and middle DTI-ALPS ($P < 0.001$); and weaker anterior BOLD-CSF coupling ($P < 0.05$) than HCs after controlling for cortical gray matter volume in both datasets. In bvFTD from the discovery dataset, the anterior DTI-ALPS was negatively associated with the expression of the bvFTD-related metabolic pattern ($r = -0.52$, $P = 0.034$) and positively related with regional standardized uptake value ratios of

Corresponding author: Liyong Wu or Min Chu, Department of Neurology, Xuanwu Hospital, Capital Medical University, Changchun Street 45, Beijing, China; wmywly@hotmail.com or cmsddhr@sina.com.

*Equal contribution

†Data used in the replication dataset of this article were obtained from the Frontotemporal Lobar Degeneration Neuroimaging Initiative (FTLDNI) database. The investigators at NIFD/FTLDNI contributed to the design and implementation of FTLDNI and/or provided data but did not participate in analysis or writing of this report (unless otherwise listed, http://4rtniftldni.ini.usc.edu/).

Author contributions

DJ, MC, and LW contributed to the conception and design of the study; DJ, LL, YK, and MC contributed to the acquisition and analysis of data; DJ, ZC, PR, KC, LR, MC, and LW contributed to drafting the text or preparing the figures.

Potential Conflicts of Interest

The authors have no conflicts of interest to declare.

^{18}F-FDG-PET in bvFTD-related brain regions (r = 0.49–0.62, P range: 0.017–0.047). Anterior and middle glymphatic function were related to global cognition and disease severity.

Interpretation: Our findings reveal abnormal glymphatic function, especially in the anterior and middle regions of brain in bvFTD. Regional glymphatic dysfunction may contribute to the pathogenesis of bvFTD.

Keywords

Behavioral variant frontotemporal dementia; glymphatic system; metabolic pattern

Introduction

Frontotemporal dementia (FTD) is the third most common neurodegenerative dementia characterized by predominant involvement in the frontal and/or temporal lobes. The behavioral variant of FTD (bvFTD) is the most prevalent clinical phenotype of FTD, presenting with progressive deficits in personal and social behavior, such as apathy and disinhibition.[1] The pathogenetic mechanism of FTD is believed to be driven by the cortical and subcortical accumulation of aberrant proteins, including mainly microtubule-associated protein tau, TAR DNA-binding protein 43 (TDP-43), and fused-in-sarcoma.[1–4] Insufficient glymphatic clearance may play a significant role in the accumulation and spread of neurotoxic proteins.[5] The glymphatic system is a recently discovered brain extracellular clearance system that involves multiple complex steps, including CSF and interstitial fluid (ISF) production and movement of glymphatic fluid.[6,7] Figure 1A summarizes the structure of glymphatic systems. Notably, animal studies have uncovered that the glymphatic pathway may have different clearance rates in different brain regions and drive CSF-ISF bidirectionally from the “watershed area” into either the ventricles or subarachnoid spaces.[7–10]

Indirect evidence supports the close link between the glymphatic system and bvFTD. First, TDP-43 and tau are the common pathological proteins in bvFTD.[11] Glymphatic dysfunction has been observed in TDP-43 mice.[12] Both animal studies[8,10] and in vivo human neuroimaging studies[13] have reported a close association between tau deposition and glymphatic failure. More importantly, the topographic pattern of bvFTD[14,15] and the apathy- and disinhibition-related regions[16] mainly involve the anterior cingulate, frontal lobe, insula, and striatum. Invasive studies to evaluate the glymphatic system have reported that intrathecally-delivered contrast agents initially inflow into the cingulate cortex, mediobasal frontal lobe, insula, and limbic structures, and remain trapped in the same regions.[17,18] The pattern of glymphatic inflow overlap with the topographic pattern of bvFTD (Fig. 1B). This spatial correlation suggests that glymphatic impairment, especially in local brain regions, may be responsible for the pathogenesis of bvFTD. Therefore, we hypothesized that the glymphatic function is impaired in bvFTD and regional glymphatic failure may contribute to the topographic pattern and clinical symptom of bvFTD.

Several noninvasive neuroimaging proxies have been used singly but not in combination to evaluate glymphatic function in some neurodegenerative diseases (e.g. Alzheimer’s disease and Parkinson’s disease) but not yet in bvFTD, including choroid plexus (CP) volume as

a surrogate marker for CSF production (Fig. 2A),[19,20] diffusion tensor imaging along the perivascular space (DTI-ALPS) index near the lateral ventricles for subcortical glymphatic movement (Fig. 2B),[13,21–24] and the coupling between blood-oxygen-level-dependent (BOLD) signals from cortical gray matter and CSF signals (BOLD-CSF coupling) for cortical glymphatic movement (Fig. 2C).[25,26]

To comprehensively investigate the function of the glymphatic system in patients with bvFTD, the above three noninvasive neuroimaging proxies were used in this study. To evaluate regional glymphatic function, DTI-ALPS and BOLD-CSF coupling were further divided into anterior, middle, and posterior regions (Fig. 2B, C). The topographic pattern of bvFTD was identified by SSM/PCA analysis of ^{18}F-FDG-PET scans. Then, we correlated these measures to neuropsychological assessments, disease-related metabolic pattern, and the metabolic activity in bvFTD-related brain regions.

Materials and methods

Participants

The research was conducted in accordance with the principles of the Declaration of Helsinki and was approved by the Ethics Committees of Xuanwu Hospital, Capital Medical University. Written informed consent was obtained from all participants or their legal guardians. To validate the reproducibility of the results, data used in this study were obtained from two independent cohorts (discovery and replication datasets) consisting of patients with bvFTD and healthy controls (HCs), who were matched for age and sex within each dataset. The discovery dataset consisted of 26 bvFTD and 29 HCs who enrolled from July 1, 2017, to August 31, 2021, at the Department of Neurology, Xuanwu Hospital. All participants underwent neuropsychological assessments, and brain ^{18}F-FDG PET/MRI scans. The replication dataset included 48 patients with bvFTD, and 38 HCs from the frontotemporal lobar degeneration neuroimaging initiative (FTLDNI) project initiated in 2010 and funded by the National Institute of Aging. The included patients received comprehensive neuropsychological assessments and multimodal MRI scans (including 3D T1-weighted sagittal scan, DTI scans with b = 1000 s/mm^2, and resting-state fMRI (rsfMRI) scans) on the same day. Data was accessed and downloaded through the Laboratory of Neuroimaging Image Data Archive (LONI) on March 7th, 2023. Updated information on participation and protocol can be obtained from http://memory.ucsf.edu/research/studies/nifd. The inclusion criteria for patients with bvFTD patients from these datasets fulfilled the 2011 consensus possible or probable bvFTD consortium criteria.[27]

Neuropsychological assessments

For neuropsychological assessments, memory, language, and behavioral abnormalities were evaluated. The Mini-mental State Examination (MMSE) and the Montreal Cognitive Assessment (MoCA) were used to assess global cognitive level.[28,29] The Clinical Dementia Rating (CDR) scale was used to describe disease severity.[30] Word-list memory was evaluated using Rey's Auditory Verbal Learning Test (AVLT) in the discovery dataset and California Verbal Learning Test (CVLT) in the replication dataset.[31,32] Language was evaluated using the Boston Naming Test (BNT).[33] The severity of behavioral abnormalities

was assessed using the Neuropsychiatry Inventory Questionnaire (NPI-Q; including the total score, apathy severity score, and disinhibition severity score),[34] and the Frontal Behavior Inventory (FBI) which was divided into the negative apathy symptom subscale (first 12 items) and the positive disinhibition symptom subscale (last 12 items).[35]

MRI acquisition

In the discovery dataset, all participants underwent a multimodal brain MRI session using a hybrid 3.0 T time-of-flight PET/MRI scanner (SIGNA PET/MR, GE Healthcare, WI, USA). PET and MRI data were acquired simultaneously using a vendor-supplied 19-channel head and neck union coil. The MRI protocol included a 3D T1-weighted sagittal scan, DTI scans, rsfMRI scans, and a ^{18}F-FDG-PET scan obtained after administering 3.7 MBq/kg 18F-FDG. The acquisition parameters were as follows: i) 3D T1-weighted fast field echo sequence, repetition time (TR) = 6.9 ms, echo time (TE) = 2.98 ms, flip angle = 12°, inversion time = 450 ms, matrix size = 256 × 256, field-of-view (FOV) = 256 × 256 mm^2, slice thickness = 1 mm, 192 sagittal slices with no gap, and voxel size = 1 × 1 × 1 mm^3; ii) diffusion-weighted spin-echo echo-planar imaging sequence with 5 b-value of 0 s/mm^2 and 30 b-value of 1000 s/mm^2 along noncollinear directions, TR = 16500 ms, TE = 74.6 ms, matrix size= 112 × 112, FOV = 256 × 256 mm^2, slice thickness = 2 mm, 70 axial slices with no slice gap, and number of excitations = 1; iii) rsfMRI with an echo-planar image sequence, TR = 2000 ms, TE = 30 ms, flip angle = 90°, partial resolution =3.6 × 3.6 × 4.4 mm, slice thickness = 3.6 mm, and 240-time slices. iv) static ^{18}F-FDG-PET, matrix size = 192 × 192, FOV = 350 × 350 mm^2, and pixel size = 1.82 × 1.82 × 2.78 mm^3, with corrections for random coincidences, dead time, scatter, and photon attenuation. During the MRI scanning session, foam pads were used inside the head coil to reduce potential head motion.

In the replication dataset, multimodal MRI images were acquired on a 3T Siemens [Munich, Germany] Tim Trio at the University of California San Francisco or a 3T General Electric (Boston, MA) MRI at Mayo Clinic. The MRI protocol included a 3D T1-weighted sagittal scan, DTI scans with b = 1000 s/mm^2, and rsfMRI scans. Participants from Mayo Clinic site also had an ^{18}FDG-PET scan on a GE Discovery RX PET/CT. The acquisition parameters were obtained in the LONI at ida.loni.usc.edu.

CP segmentation

The volume of the CP, the primary site of CSF secretion, has been speculated to be an indirect imaging marker for evaluating CSF production and toxic clearance.[19,20] Automated segmentation of the CP within the lateral ventricles was obtained from the T1-weighted MRI sequence using the t1-freesurfer pipeline of Clinica 0.7.1 (https://www.clinica.run/; Fig. 2A).[36] The CP segmentation was thoroughly examined and corrected manually when needed by one neurologist, these manually corrected CP maps were quality-checked independently and finalized by a second neurologist. Total intracranial volume (ICV), cortical gray matter volume and CP volume were extracted. To reduce inter-participant variability, CP volume was expressed as the ratio of CP volume to ICV, as described previously.[20]

Quantification of DTI-ALPS

DTI-ALPS index is used to evaluate water diffusivity along the perivascular spaces (PVS) of the medullary veins at the level of the lateral ventricle, which primarily reflects the brain's ability to drive fluids from subcortical region into the lateral ventricles.[13,21–24] To obtain water diffusivity values along the PVS, diffusivity values along the x-, y-, and z-axes would extract from both projection fibers (Dx^{proj}, Dy^{proj}, Dz^{proj}) and association fibers (Dx^{assoc}, Dy^{assoc}, and Dz^{assoc}) at the same level of the lateral ventricle. The projection fibers that run in the direction of the *z*-axis pass along the wall of the lateral ventricle and are adjacent to the association fibers that run in the direction of the *y*-axis. The diffusivity of PVS can be reflected by the major difference in water molecule behavior between x-axis diffusivity in both fibers (Dx^{proj} and Dx^{assoc}) and diffusivity which runs perpendicular to them (Dy^{proj} and Dz^{assoc}). Specifically, the DTI-ALPS index presents this relationship and is defined as follows:[21]

$$DTI-ALPS\,index = mean(Dxproj, Dxassoc)/mean(Dyproj, Dzassoc)$$

The pre-processing of diffusion-weighted images was performed using the dwi-preprocessing-using-t1 pipeline and dwi-dti pipeline of Clinica 0.7.1.[36] Specifically, the DWIs were processed including correction for eddy current-induced distortions, participant movements, susceptibility induced distortions, and bias field.[37] The fractional anisotropy (FA) map of each subject was registered to the FA map of the JHU atlas template with the ANTs SyN algorithm,[38] and the estimated nonlinear deformation was applied to other diffusion metric maps to obtain all DTI-based maps in the space of the JHU atlas (spatial resolution, $1 \times 1 \times 1$ mm^3).[39–41] The accuracy of coregistration was confirmed visually and found no need to do any manual correction. The regions of interest (ROIs) with a thickness of 3mm were extracted within the left projection (anterior, superior, and posterior corona radiata) and association fiber (superior longitudinal fasciculus) at the level of the lateral ventricle (MNI coordinates z = 26) based on the atlas labels, and then the global DTI-ALPS (gDTI-ALPS) was computed. These ROIs were further segmented into anterior, middle, and posterior parts to calculate the anterior DTI-ALPS (aDTI-ALPS), middle DTI-ALPS (mDTI-ALPS), and posterior DTI-ALPS (pDTI-ALPS), respectively. To further explore the glymphatic gradient, $3 \times 3 \times 3$ mm^3 cubic ROIs were placed at 1mm intervals from anterior to posterior at the same level. A total of 46 pairs of cubic ROIs were generated and relevant DTI-ALPS were calculated (Fig. 2B). Due to the potential impact of white matter pathology on DTI-ALPS,[22] we further evaluated the white matter lesion. The volume of white matter lesion (WML) was extracted from the original FLAIR sequence using the Lesion Segmentation Toolbox in Statistical Parametric Mapping 12 (https://www.statistical-modelling.de/lst.html).

Coupling between BOLD Signal and CSF Flow

The large cortical BOLD signal has been reported to be accompanied by strong CSF movement, which possibly indicates cortical glymphatic function.[25,26] To obtain BOLD-CSF coupling, the pre-processing of rsfMRI images was performed using the 1000 Functional Connectomes Project script (version 1.1-beta) with a minor modification.[42] Each raw rsfMRI data sequentially underwent dropping of the first five volumes, skull

stripping, and slice-timing correction. For the extraction of the CSF signal, rsfMRI data underwent high-pass filtering (0.01–0.1 Hz) and linear and quadratic detrending, but without motion correction. Due to the movement of tissue in and out of the imaging volume, accurate motion correction cannot be achieved for edge slices.[43] For analyzing global BOLD (gBOLD) effects, rsfMRI data underwent motion correction, high-pass filtering (0.01–0.1 Hz), linear and quadratic detrending, and spatial Gaussian kernel smoothing (full-width at maximum, 4 mm). To avoid spatial blurring, all fMRI signal analyses were performed in the original spatial frame without transforming to a standard space.[43] The gBOLD signal was extracted from the cortical gray matter region of the cerebrum which was defined based on the automated anatomical labelling 2 (AAL2) atlases.[44] To assess the regional distribution of glymphatic function, the AAL2 atlas was divided into the anterior, middle, and posterior parts based on the labels of the frontal, temporoparietal, and occipital regions (Fig. 2C; yellow, blue, and red mask, respectively). The CSF signals were identified from the edge slice of fMRI acquisition located between the upper spinal cord/medulla oblongata and lower cerebellum, which was expected to have maximal sensitivity to inflow effects.[43,45] Then, the mean timeseries of CSF were extracted based on the signal intensity for each participant (Fig. 2D).

To quantify the gBOLD-CSF coupling, the cross-correlation function was calculated between the gBOLD and CSF signals at various time lags (from −20 to 20s). The correlation coefficients from the negative peaks at lags of +2 and +3 s for the discovery and replication datasets, respectively, were used to quantify the strength of gBOLD-CSF coupling for each participant (Fig. 3).[25,26] Moreover, the cross-correlation function between the negative first-order derivative of the gBOLD signal and the CSF signal was calculated, as described.[25,43] To check the significance of the correlation value at 95% confidence interval, gBOLD and CSF signals from different participants were randomly matched and correlation was calculated across random pairs 1000 times repeatedly.[25] In addition, the cross-correlation function between CSF signals and the anterior, middle, and posterior BOLD signals was calculated to obtain coupling correlation coefficients, named aBOLD-CSF, mBOLD-CSF, and pBOLD-CSF couplings, respectively.

FDG-PET preprocessing and metabolic covariance pattern of bvFTD

The pre-processing of PET images was performed using the pet-volume pipeline of Clinica 0.7.1.[36,46] The PET image is spatially normalized into Montreal Neurological Institute space using the DARTEL deformation model, and intensity normalized using the average PET uptake in pons reference region. As in previous studies,[15] SSM/PCA was applied to the ^{18}F-FDG PET data of 26 patients with bvFTD and 29 age- and sex-matched HCs from the discovery dataset to identify the metabolic covariance pattern of bvFTD, also called the bvFTD-related pattern (bvFTD-RP), and quantify the expression values for bvFTD-RP. This pattern was validated by computing its expression in 14 patients and 5 age- and sex-matched HCs from the replication dataset. Finally, standardized uptake value ratios (SUVRs) from ^{18}F-FDG PET images were computed for a set of regions obtained from Hammers' brain atlas.[47] Based on this atlas and the bvFTD-RP, nine ROIs were selected, including bilateral thalamus, caudate, insular, anterior and posterior cingulate gyri (ACC and PCC), orbitofrontal cortex (OFC), rectus gyrus, frontal lobe, and temporal lobe.

Statistical analysis

All statistical analyses were performed with the R Statistics software (version 4.1.3). Two-sample *t-test* or Mann–Whitney *U* test for continuous variables and χ^2 test for categorical variables were performed whenever appropriate for between-group comparisons. We repeated between-group comparisons of glymphatic measures after controlling for cortical gray matter volume of the whole cerebrum. We further controlled for WML and ICV in the DTI-ALPS inter-group comparison. Partial correlation analysis was conducted to evaluate the relationship between glymphatic measures and bvFTD-RP expression and mean regional SUVRs value in nine ROIs from the ^{18}F-FDG-PET images, with age, sex and frontotemporal volume as control variables and correction for multiple comparisons using the false discovery rate (FDR) approach. Regression analyses were performed in bvFTD to assess the associations between glymphatic measures and neuropsychological test scores adjusted for age, sex, years of education, frontotemporal volume in the discovery dataset, and further adjusted for the scanning sites in the replication dataset and the pooled data. Finally, relationship between glymphatic measures was evaluated in the whole cohort and in the groups separately. Specifically, the paired-sample *t-test* was performed between aDTI-ALPS and pDTI-ALPS, and aBOLD-CSF coupling and pBOLD-CSF coupling; partial correlation analyses were performed to examine the relationship between CP, DTI-ALPS, and BOLD-CSF coupling, with age, sex and scanning sites as control variables. *P*-value < 0.05 was considered statistically significant.

Results

Demographic and clinical features

Table 1 summarizes the demographic and clinical information of the patients with bvFTD and HCs. HCs were age- and sex-matched with the patients with bvFTD ($P > 0.104$) and no significant group differences were found in education years and ICV in both datasets ($P > 0.051$). Patients with bvFTD had lower cortical gray matter volume, WML, MMSE, MoCA, BNT, and AVLT/CVLT scores (all $P < 0.001$) than HCs. Patients from the replication dataset had higher education years, ICV, and MMSE, NPI-Q scores than those from the discovery dataset ($P \leq 0.009$).

Between-group comparisons of CP volume, DTI-ALPS, and BOLD-CSF coupling

Table 2 shows the result of between-group comparisons of CP volume, DTI-ALPS, and BOLD-CSF coupling. Patients with bvFTD had higher CP volume (ratio of ICV× 10^3) than HCs in both datasets (all $P < 0.001$). In the discovery dataset, patients with bvFTD showed lower aDTI-ALPS ($P = 0.015$) and mDTI-ALPS ($P < 0.001$) than HCs; however, after controlling for the WML and ICV, there was no difference between the groups in DTI-ALPS. In the replication dataset, patients with bvFTD showed lower DTI-ALPS than HCs (all $P \leq 0.004$). Similar results were also observed based on DTI-ALPS calculating from cubic ROIs (Fig. 6A, B).

A strong coupling between global cerebral cortex activity and CSF flow was observed in both dataset despite a small difference and the pattern is similar to the results of previous studies (Fig. 3).[25,43] The mean gBOLD-CSF cross-correlation function displayed a positive

peak (r range: 0.21–0.24, all $P < 0.001$) at time lags from −2 to −3 s and a negative peak (r range: −0.19–−0.24, all $P < 0.001$) at time lags of 2–3 s in both datasets. The cross-correlation function between the negative first-order derivative of the gBOLD signal and the CSF signal had a large positive peak at time lags of 0 s (r range: 0.22−0.35, $P < 0.001$). Patients with bvFTD had significantly weaker gBOLD-CSF, aBOLD-CSF, mBOLD-CSF, and pBOLD-CSF coupling than HCs in both datasets (P range: 0.029–0.001). After controlling for cortical gray matter volume, only aBOLD-CSF remained statistically different in both datasets (P range: 0.045–0.016; Table 2).

Correlation between regional glymphatic function and metabolic pattern

Spatial covariance analysis of ^{18}F-FDG PET images from the discovery dataset revealed significant bvFTD-RP (principal component 1, accounting for 36.2% of the participant × voxel variance). The topography of bvFTD-RP was mainly characterized by bilateral metabolic reductions in the thalamus, caudate, insular, ACC, OFC, rectus gyrus, inferior and middle frontal gyrus, and temporopolar (Fig. 4A). These findings are similar to those from another study.[15] The expression value of this pattern significantly separated the patients with bvFTD from HCs in the discovery dataset ($P < 0.001$; Student's t-tests; Fig. 4B) and was validated in the replication dataset ($P < 0.001$; Fig. 4D). A significant negative correlation was observed between the aDTI-ALPS score and a higher bvFTD-RP expression value in patients with bvFTD ($r = -0.52$, FDR-corrected $P = 0.035$) in the discovery dataset. No significant correlation was found between the bvFTD-RP expression value and other glymphatic measures (all $P > 0.069$; Fig. 4C, E).

CP volume had a significant correlation with regional metabolic SUVRs of the caudate (r = −0.56−−0.71, FDR-adjusted P value = 0.046−0.048) in both datasets. Furthermore, in the discovery dataset, significant positive associations were observed between aDTI-ALPS and regional metabolic SUVRs of the frontal lobe ($r = 0.49$, FDR-adjusted P value = 0.047), rectus gyrus ($r = 0.55$, FDR-corrected P value = 0.034), and OFC ($r = 0.62$, FDR-corrected P = 0.017; Fig. 4C) However, no significant correlation was found between regional metabolic SUVRs and BOLD-CSF in both datasets nor DTI-ALPS in the replication dataset (Fig. 4E).

Correlation between glymphatic function and neuropsychological scores

In patients with bvFTD from the pooled data, CP volume had a significant correlation with MMSE (unstandardized $\beta = -0.024$, $P < 0.001$), CDR-SOB (unstandardized β = 0.043, $P < 0.001$), and NPI apathy (unstandardized $\beta = 0.061$, $P = 0.003$) scores. In addition, aDTI-ALPS and mDTI-ALPS was associated with MMSE score (all unstandardized β = 0.008, all $P = 0.003$) and CDR-SOB score (unstandardized β = −0.008 and −0.009, P = 0.040 and 0.014, respectively). A positive correlation was found between the value of aBOLD-CSF coupling and CDR-SOB score (unstandardized $\beta = 0.013$, $P = 0.019$). Details for other results are provided in Figure 5.

Relationship between glymphatic measures

In both groups, aDTI-ALPS was higher than pDTI-ALPS (all $P < 0.001$), whereas aBOLD-CSF coupling was lower than pBOLD-CSF coupling (all $P < 0.001$; Fig. 6C, D). In addition,

gDTI-ALPS showed a negative correlation with CP volume ($r = -0.28$, $P < 0.001$) and gBOLD-CSF coupling ($r = -0.19$, $P = 0.025$; Fig. 6E) in all subjects.

Discussion

In this study, we used a multi-parametric segmentation approach to comprehensively evaluate glymphatic function and its regional distribution in patients with bvFTD from two independent cohorts. Three noninvasive neuroimaging proxies, including CP volume, DTI-ALPS, and BOLD-CSF coupling, were used as surrogate markers for CSF production, subcortical glymphatic movement and cortical glymphatic movement, respectively. The relationship between glymphatic function and bvFTD-related metabolic pattern and clinical symptoms was investigated. The findings of this study suggest that glymphatic function, especially in forebrain and midbrain are impaired in patients with bvFTD. Moreover, glymphatic function has a spatial correlation with the bvFTD-related metabolic pattern and clinical symptoms.

This study suggests that the glymphatic system, including the CSF production and the glymphatic movement, is impaired in patients with bvFTD. First, patients with bvFTD showed higher CP volume than HCs. A larger CP volume is speculated to potentially boost CSF production by increasing functional units, which in turn may offset glymphatic dysfunction and enhance waste clearance.[19,48] Notably, this study reveals that enlarged CP volume is associated with lower DTI-ALPS (Fig. 6E). This result suggests that glymphatic movement in the subcortical areas may be susceptible to changes in CSF production. Consistently, Johnson reported that improved paravascular flow is associated with decreased CP perfusion.[48] Second, patients with bvFTD showed lower aDTI-ALPS, mDTI-ALPS and weak aBOLD-CSF coupling than HCs. On the one hand, this result suggests that bidirectional glymphatic movement impairment in brain parenchyma may occur in patients with bvFTD. Although FTD presents with predominant atrophy in the frontal and temporal lobe cortex, toxic proteins deposition also occurs in multiple subcortical brain regions.[4,49] Bidirectional glymphatic flow may drain abnormal proteins from ISF into the ventricles or subarachnoid space.[50–52] Therefore, slowed glymphatic movement could lead to waste accumulation in both cortical and subcortical regions. On the other hand, this result may imply more severe forebrain and midbrain glymphatic impairment in patients with bvFTD. FTD pathology is mainly found in the forebrain and midbrain, matching the distribution of glymphatic failure in bvFTD patients.[49] Notably, in the discovery dataset, WML pathology was observed to potentially affect DTI-ALPS, which is consistent with previous research findings.[22]

In this study, a spatial correlation between regional glymphatic function and bvFTD-specific metabolic network was observed. Given that bvFTD presents with a predominant involvement in the prefrontal regions, ACC, and striatum, which seem to mostly overlap with the distribution of glymphatic influx, bvFTD may be more closely associated with glymphatic function than other neurodegenerative diseases. The findings revealed that aDTI-ALPS, but not other measures, was negatively linked with the bvFTD-RP expression value. This result indicates that regional rather than global glymphatic dysfunction may play a major role in regional protein deposition and spread and thus account for the

topographic pattern of brain metabolic reduction in neurodegenerative diseases. This study also shown that aDTI-ALPS was associated with metabolic activity in the anterior brain regions, including the frontal lobe, OFC, and rectus gyrus. Metabolic insufficiency in disease-related regions may be explained by neuronal loss due to the regional accumulation of metabolic waste and toxic proteins.[54] Cortical hypometabolism was reported to reflect tau pathology and predict TDP-43 status.[55,56] Thus, taken together, these findings suggests that regional glymphatic dysfunction may account more for the pathophysiology of bvFTD. Insufficient regional glymphatic clearance, especially in anterior brain regions may lead to the accumulation and spread of neurotoxic proteins in the prefrontal lobe, and thus contribute to bvFTD. Notably, the spatial relationship between bvFTD-RP and glymphatic function was not confirmed in the replication dataset, potentially due to the small sample size, so these findings need to be interpreted with caution.

In addition, the findings of this study confirmed that CP volume and anterior and middle glymphatic movement are related to global cognition and disease severity in patients with bvFTD. Consistent with our findings, a study found that global cognition and disease severity were associated with PVS burden, a biomarker that may indirectly reflect glymphatic function, in patients with bvFTD.[53]Additionnaly, higher CP volume was linked with higher NPI and FBI apathy scores. Apathy, the most prevalent core symptom in bvFTD,[57] is defined as a quantitative reduction of goal-directed activity.[16] Apathy-related brain regions, mainly including the prefrontal cortex, OFC, ACC, and caudate,[16] also seem to resemble the pattern of glymphatic influx (Fig. 1B). The reduced metabolic activity in these regions was observed in our study. The elevation of CSF production may induce apathy by modulating the metabolism of the corresponding brain regions, particularly the caudate (Fig. 4C, E). Our findings may indicate a clinicopathological correlation between glymphatic function and bvFTD. Caution is needed in interpreting these results as they only demonstrate a correlation. Further animal experiments are necessary to establish a causal relationship. It is worth exploring whether improving brain clearance improves key symptoms of bvFTD.

The segmentation approach of this study may reveal a physiological phenomenon that posterior cortical clearance may be stronger than anterior cortical clearance, whereas posterior subcortical clearance may be weaker than anterior subcortical clearance (Fig. 6C, D). The subcortical glymphatic gradient (Fig. 6A, B) is similar to the anterior-posterior gradient of white matter microstructural diffusivity.[58] In line with our findings, Harrison et al.[10] reported a higher clearance rate of tau in the caudal cortex compared to the rostral cortex in mice, which may be attributed to the caudal cortex receiving greater arterial input.[59] This distribution gradient difference in glymphatic function between the cortical and subcortical regions may be explained by a bidirectional complementation model (Fig. 1A, blue arrows of different sizes). Regional glymphatic movements may be interactive with each other to enhance the efficiency of waste clearance (Fig. 6E).

This study has a few limitations. First, although DTI-ALPS is closely associated with the gadolinium-enhanced glymphatic MRI method that is considered as a current gold standard for assessing glymphatic function,[60] validation studies for CP volume and BOLD-CSF coupling are lacking. Therefore, the relationship between glymphatic function and CP

volume and BOLD-CSF coupling should be explained cautiously. Second, pathological biomarkers, such as tau burden evaluated using tau-PET images, were not used to evaluate the relationship between focal proteins deposition and regional glymphatic function. Studies to establish their spatial relationship are warranted. Finally, the cross-sectional design of the study prevented exploration of temporal alteration in the spatial distribution of the clearance network. The spatiotemporal interaction in the glymphatic system is expected to be the topic of future research.

In summary, this study provided a multi-parametric approach to comprehensively evaluate the glymphatic function and regional distribution in patients with bvFTD using multimodal noninvasive imaging proxies. This study revealed glymphatic dysfunction, especially in the anterior and middle regions of brain, may be closely associated with the pathophysiology of bvFTD.

Acknowledgements

This work was supported by the National Natural Science Foundation of China (82271464 and 81971011), the Beijing Municipal Science and Technology Committee (7202060).

Parts of the data used in this study were obtained from the Frontotemporal Lobar Degeneration Neuroimaging Initiative (FTLDNI), which funded by National Institutes of Health Grant (R01 AG032306). The primary goals of FTLDNI are to identify neuroimaging modalities and methods of analysis for tracking frontotemporal lobar degeneration and to assess the value of imaging vs. other markers in diagnostic roles. The study is coordinated through the University of California, San Francisco, Memory and Aging Center. FTLDNI data are disseminated by the Laboratory for Neuro Imaging at the University of Southern California.

Data availability

The replication dataset in this study is openly available in the Laboratory of Neuroimaging Image Data Archive at ida.loni.usc.edu.

References

1. Bang J, Spina S, Miller BL. Frontotemporal dementia. Lancet. 2015;386(10004):1672–1682. [PubMed: 26595641]
2. Giannini LAA, Peterson C, Ohm D, et al. Frontotemporal lobar degeneration proteinopathies have disparate microscopic patterns of white and grey matter pathology. Acta Neuropathol Commun. 2021;9(1):30. [PubMed: 33622418]
3. Kawles A, Nishihira Y, Feldman A, et al. Cortical and subcortical pathological burden and neuronal loss in an autopsy series of FTLD-TDP-type C. Brain. 2022;145(3):1069–1078. [PubMed: 34919645]
4. Scarioni M, Gami-Patel P, Peeters CFW, et al. Psychiatric symptoms of frontotemporal dementia and subcortical (co-)pathology burden: new insights. Brain. Published online February 8, 2022:awac043.
5. Boland B, Yu WH, Corti O, et al. Promoting the clearance of neurotoxic proteins in neurodegenerative disorders of ageing. Nat Rev Drug Discov. 2018;17(9):660–688. [PubMed: 30116051]
6. Klostranec JM, Vucevic D, Bhatia KD, et al. Current Concepts in Intracranial Interstitial Fluid Transport and the Glymphatic System: Part I-Anatomy and Physiology. Radiology. 2021;301(3):502–514. [PubMed: 34665028]
7. Mestre H, Mori Y, Nedergaard M. The Brain's Glymphatic System: Current Controversies. Trends Neurosci. 2020;43(7):458–466. [PubMed: 32423764]

8. Ishida K, Yamada K, Nishiyama R, et al. Glymphatic system clears extracellular tau and protects from tau aggregation and neurodegeneration. J Exp Med. 2022;219(3):e20211275.
9. Klostranec JM, Vucevic D, Bhatia KD, et al. Current Concepts in Intracranial Interstitial Fluid Transport and the Glymphatic System: Part II-Imaging Techniques and Clinical Applications. Radiology. 2021;301(3):516–532. [PubMed: 34698564]
10. Harrison IF, Ismail O, Machhada A, et al. Impaired glymphatic function and clearance of tau in an Alzheimer's disease model. Brain. 2020;143(8):2576–2593. [PubMed: 32705145]
11. Piguet O, Kumfor F, Hodges J. Diagnosing, monitoring and managing behavioural variant frontotemporal dementia. Medical Journal of Australia. 2017;207(7):303–308. [PubMed: 28954617]
12. Zamani A, Walker AK, Rollo B, et al. Impaired glymphatic function in the early stages of disease in a TDP-43 mouse model of amyotrophic lateral sclerosis. Transl Neurodegener. 2022;11(1):17. [PubMed: 35287738]
13. Hsu JL, Wei YC, Toh CH, et al. MRI images implicate glymphatic alterations mediate cognitive dysfunction in AD. Ann Neurol. Published online October 10, 2022.
14. Perry DC, Brown JA, Possin KL, et al. Clinicopathological correlations in behavioural variant frontotemporal dementia. Brain. 2017;140(12):3329–3345. [PubMed: 29053860]
15. Nazem A, Tang CC, Spetsieris P, et al. A multivariate metabolic imaging marker for behavioral variant frontotemporal dementia. Alzheimers Dement (Amst). 2018;10:583–594. [PubMed: 30417069]
16. Jenkins LM, Wang L, Rosen H, Weintraub S. A transdiagnostic review of neuroimaging studies of apathy and disinhibition in dementia. Brain. Published online April 7, 2022:awac133.
17. Ringstad G, Vatnehol SAS, Eide PK. Glymphatic MRI in idiopathic normal pressure hydrocephalus. Brain. 2017;140(10):2691–2705. [PubMed: 28969373]
18. Nedergaard M, Goldman SA. Glymphatic failure as a final common pathway to dementia. Science. 2020;370(6512):50–56. [PubMed: 33004510]
19. Tadayon E, Pascual-Leone A, Press D, Santarnecchi E, Alzheimer's Disease Neuroimaging Initiative. Choroid plexus volume is associated with levels of CSF proteins: relevance for Alzheimer's and Parkinson's disease. Neurobiol Aging. 2020;89:108–117. [PubMed: 32107064]
20. Choi JD, Moon Y, Kim HJ, Yim Y, Lee S, Moon WJ. Choroid Plexus Volume and Permeability at Brain MRI within the Alzheimer Disease Clinical Spectrum. Radiology. Published online May 17, 2022:212400.
21. Taoka T, Masutani Y, Kawai H, et al. Evaluation of glymphatic system activity with the diffusion MR technique: diffusion tensor image analysis along the perivascular space (DTI-ALPS) in Alzheimer's disease cases. Jpn J Radiol. 2017;35(4):172–178. [PubMed: 28197821]
22. Kamagata K, Andica C, Takabayashi K, et al. Association of MRI Indices of Glymphatic System With Amyloid Deposition and Cognition in Mild Cognitive Impairment and Alzheimer Disease. Neurology. Published online September 19, 2022:10.1212/WNL.0000000000201300.
23. Steward CE, Venkatraman VK, Lui E, et al. Assessment of the DTI-ALPS Parameter Along the Perivascular Space in Older Adults at Risk of Dementia. J Neuroimaging. 2021;31(3):569–578. [PubMed: 33556226]
24. Ma X, Li S, Li C, et al. Diffusion Tensor Imaging Along the Perivascular Space Index in Different Stages of Parkinson's Disease. Front Aging Neurosci. 2021;13:773951. [PubMed: 34867300]
25. Han F, Brown GL, Zhu Y, et al. Decoupling of Global Brain Activity and Cerebrospinal Fluid Flow in Parkinson's Disease Cognitive Decline. Mov Disord. 2021;36(9):2066–2076. [PubMed: 33998068]
26. Han F, Chen J, Belkin-Rosen A, et al. Reduced coupling between cerebrospinal fluid flow and global brain activity is linked to Alzheimer disease-related pathology. PLoS Biol. 2021;19(6):e3001233.
27. Rascovsky K, Hodges JR, Knopman D, et al. Sensitivity of revised diagnostic criteria for the behavioural variant of frontotemporal dementia. Brain. 2011;134(Pt 9):2456–2477. [PubMed: 21810890]

28. Folstein MF, Folstein SE, McHugh PR. “Mini-mental state”. A practical method for grading the cognitive state of patients for the clinician. J Psychiatr Res. 1975;12(3):189–198. [PubMed: 1202204]
29. Nasreddine ZS, Phillips NA, Bédirian V, et al. The Montreal Cognitive Assessment, MoCA: a brief screening tool for mild cognitive impairment. J Am Geriatr Soc. 2005;53(4):695–699. [PubMed: 15817019]
30. Morris JC. The Clinical Dementia Rating (CDR): current version and scoring rules. Neurology. 1993;43(11):2412–2414.
31. Schmidt M Rey Auditory Verbal Learning Test A Handbook. Published online 1996. Accessed March 18, 2023. http://cirrie.buffalo.edu/database/20810/
32. Elwood RW. The California Verbal Learning Test: psychometric characteristics and clinical application. Neuropsychol Rev. 1995;5(3):173–201. [PubMed: 8653108]
33. Guo QH. Boston Naming Test in Chinese Elderly, Patient with Mild Cognitive Impairment and Alzheimer’s Dementia. Chinese Mental Health Journal. Published online 2006. Accessed March 18, 2023. http://en.cnki.com.cn/Article_en/CJFDTOTAL-ZXWS200602002.htm
34. Cummings JL, Mega M, Gray K, Rosenberg-Thompson S, Carusi DA, Gornbein J. The Neuropsychiatric Inventory: comprehensive assessment of psychopathology in dementia. Neurology. 1994;44(12):2308–2314. [PubMed: 7991117]
35. Kertesz A, Davidson W, Fox H. Frontal behavioral inventory: diagnostic criteria for frontal lobe dementia. Can J Neurol Sci. 1997;24(1):29–36. [PubMed: 9043744]
36. R A, B N, D M, et al. Clinica: An Open-Source Software Platform for Reproducible Clinical Neuroscience Studies. Frontiers in neuroinformatics. 2021;15.
37. Wen J, Samper-González J, Bottani S, et al. Reproducible Evaluation of Diffusion MRI Features for Automatic Classification of Patients with Alzheimer’s Disease. Neuroinformatics. 2021;19(1):57–78. [PubMed: 32524428]
38. Avants BB, Epstein CL, Grossman M, Gee JC. Symmetric diffeomorphic image registration with cross-correlation: evaluating automated labeling of elderly and neurodegenerative brain. Med Image Anal. 2008;12(1):26–41. [PubMed: 17659998]
39. Yokota H, Vijayasarathi A, Cekic M, et al. Diagnostic Performance of Glymphatic System Evaluation Using Diffusion Tensor Imaging in Idiopathic Normal Pressure Hydrocephalus and Mimickers. Curr Gerontol Geriatr Res. 2019;2019:5675014. [PubMed: 31320896]
40. Siow TY, Toh CH, Hsu JL, et al. Association of Sleep, Neuropsychological Performance, and Gray Matter Volume With Glymphatic Function in Community-Dwelling Older Adults. Neurology. 2022;98(8):e829–e838. [PubMed: 34906982]
41. Wakana S, Jiang H, Nagae-Poetscher LM, van Zijl PCM, Mori S. Fiber tract-based atlas of human white matter anatomy. Radiology. 2004;230(1):77–87. [PubMed: 14645885]
42. Biswal BB, Mennes M, Zuo XN, et al. Toward discovery science of human brain function. Proc Natl Acad Sci U S A. 2010;107(10):4734–4739. [PubMed: 20176931]
43. Fultz NE, Bonmassar G, Setsompop K, et al. Coupled electrophysiological, hemodynamic, and cerebrospinal fluid oscillations in human sleep. Science. 2019;366(6465):628–631. [PubMed: 31672896]
44. Rolls ET, Joliot M, Tzourio-Mazoyer N. Implementation of a new parcellation of the orbitofrontal cortex in the automated anatomical labeling atlas. NeuroImage. 2015;122:1–5. [PubMed: 26241684]
45. Gao JH, Liu HL. Inflow effects on functional MRI. Neuroimage. 2012;62(2):1035–1039. [PubMed: 22019882]
46. Samper-González J, Burgos N, Bottani S, et al. Reproducible evaluation of classification methods in Alzheimer’s disease: Framework and application to MRI and PET data. Neuroimage. 2018;183:504–521. [PubMed: 30130647]
47. Hammers A, Allom R, Koepp MJ, et al. Three-dimensional maximum probability atlas of the human brain, with particular reference to the temporal lobe. Hum Brain Mapp. 2003;19(4):224–247. [PubMed: 12874777]

48. Johnson SE, McKnight CD, Lants SK, et al. Choroid plexus perfusion and intracranial cerebrospinal fluid changes after angiogenesis. J Cereb Blood Flow Metab. 2020;40(8):1658–1671. [PubMed: 31500523]

49. Giannini LAA, Peterson C, Ohm D, et al. Frontotemporal lobar degeneration proteinopathies have disparate microscopic patterns of white and grey matter pathology. Acta Neuropathol Commun. 2021;9(1):30. [PubMed: 33622418]

50. Bedussi B, van Lier MGJTB, Bartstra JW, et al. Clearance from the mouse brain by convection of interstitial fluid towards the ventricular system. Fluids Barriers CNS. 2015;12:23. [PubMed: 26435380]

51. Han H, Shi C, Fu Y, et al. A novel MRI tracer-based method for measuring water diffusion in the extracellular space of the rat brain. IEEE J Biomed Health Inform. 2014;18(3):978–983. [PubMed: 24808229]

52. Arbel-Ornath M, Hudry E, Eikermann-Haerter K, et al. Interstitial fluid drainage is impaired in ischemic stroke and Alzheimer's disease mouse models. Acta Neuropathol. 2013;126(3):353–364. [PubMed: 23818064]

53. Moses J, Sinclair B, Schwartz DL, et al. Perivascular spaces as a marker of disease severity and neurodegeneration in patients with behavioral variant frontotemporal dementia. Front Neurosci. 2022;16:1003522. [PubMed: 36340772]

54. Turner DA. Contrasting Metabolic Insufficiency in Aging and Dementia. Aging Dis. 2021;12(4):1081–1096. [PubMed: 34221551]

55. Strom A, Iaccarino L, Edwards L, et al. Cortical hypometabolism reflects local atrophy and tau pathology in symptomatic Alzheimer's disease. Brain. 2021;145(2):713–728.

56. Buciuc M, Botha H, Murray ME, et al. Utility of FDG-PET in diagnosis of Alzheimer-related TDP-43 proteinopathy. Neurology. 2020;95(1):e23–e34. [PubMed: 32518145]

57. Le Bouc R, Borderies N, Carle G, et al. Effort avoidance as a core mechanism of apathy in frontotemporal dementia. Brain. Published online November 19, 2022:awac427.

58. S Ev, R T, P A. Longitudinal study of callosal microstructure in the normal adult aging brain using quantitative DTI fiber tracking. Developmental neuropsychology. 2010;35(3).

59. Xiong B, Li A, Lou Y, et al. Precise Cerebral Vascular Atlas in Stereotaxic Coordinates of Whole Mouse Brain. Front Neuroanat. 2017;11:128. [PubMed: 29311856]

60. Zhang W, Zhou Y, Wang J, et al. Glymphatic clearance function in patients with cerebral small vessel disease. Neuroimage. 2021;238:118257.

Summary for Social Media If Published

If you and/or a co-author has a Twitter handle that you would like to be tagged, please enter it here.

We have no Twitter handle.

What is the current knowledge on the topic?

The glymphatic system is reportedly impaired in several neurodegenerative diseases, but has not yet been explored in behavioral variant frontotemporal dementia. The spatial correlation between regional glymphatic function and bvFTD remain unknown.

What question did this study address?

We aim to evaluate glymphatic function and its regional distribution in behavioral variant frontotemporal dementia and explore its association with the disease-related metabolic pattern and clinical symptoms.

What does this study add to our knowledge?

We found that glymphatic function, especially in the anterior and middle regions of brain, are impaired in behavioral variant frontotemporal dementia (bvFTD). Moreover, regional glymphatic function shows a spatial correlation with the bvFTD-related metabolic pattern and clinical symptoms.

How might this potentially impact on the practice of neurology?

Our findings support that regional glymphatic dysfunction may contribute to the pathogenesis of behavioral variant frontotemporal dementia.

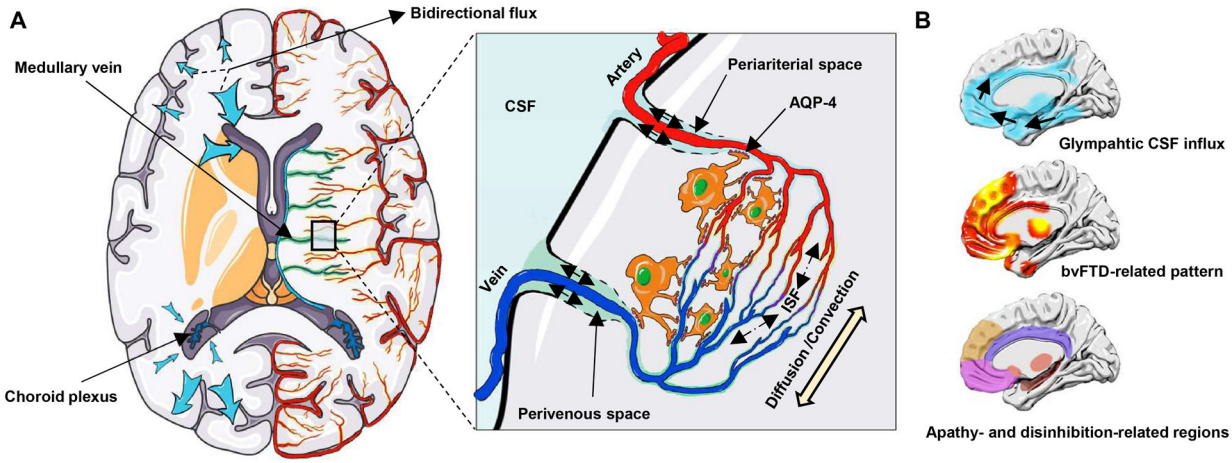

Figure 1: Glymphatic system and the spatial correlation with bvFTD.

(**A**) Choroid plexuses secret CSF. CSF inflows from periarterial spaces to the brain parenchyma, mixes with ISF by the diffusion and convection movement, and then outflows through perivenous spaces, which is facilitated by AQP-4 water channels on astroctytic end-feet. The glymphatic pathway may have different clearance rates in different brain regions and may drive CSF-ISF bidirectionally into either the ventricles or subarachnoid space (blue arrow). (**B**) Spatial correlation between the glymphatic CSF influx and bvFTD related pattern, and apathy- and disinhibition-related brain regions. The bvFTD-related pattern is identified from the discovery dataset by the multivariate spatial covariance analysis based on ^{18}F-FDG-PET imaging data. bvFTD = behavioral variant frontotemporal dementia; CSF = cerebrospinal fluid; ISF = interstitial fluid.

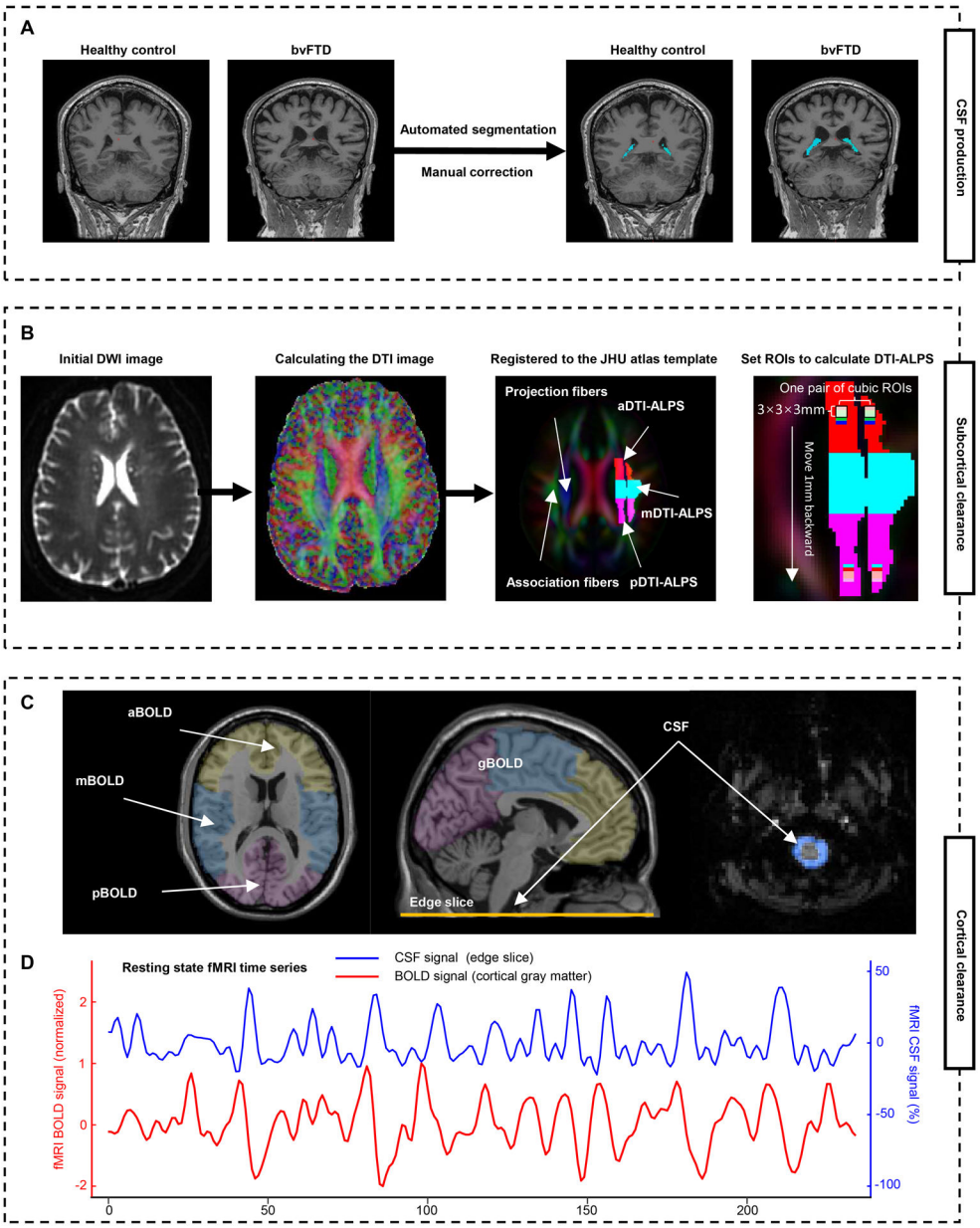

Figure 2: Schematic of the multi-parametric assessment approaches for the glymphatic function.

(**A**) Automated segmentation and manual correction of choroid plexus within the lateral ventricles. (**B**) MRI processing approach for DTI-ALPS calculation and segmentation. Initial DWI image is coregistered to the corresponding T1-weighted image, and then calculated the DTI image. The FA map is registered to the FA map of the JHU atlas template. The ROIs were extracted and segmented into three parts based on the atlas labels (anterior, superior, and posterior corona radiata, and superior longitudinal fasciculus). Additionally, 46 parts of $3 \times 3 \times 3$ mm^3 cubic ROIs are drawn in the left projection and association fibers. (**C**) To calculate the BOLD-CSF coupling, the global BOLD signal is extracted from the cortical gray matter region of cerebrum, then is divide into three parts: anterior BOLD, middle BOLD, and posterior BOLD. The CSF signals are extracted from the edge

slice of fMRI acquisition located between the upper spinal cord/medulla oblongata and lower cerebellum. (**D**) A strong coupling between the global cortical BOLD signals and CSF signals was observed in a representative healthy control. a/m/pDTI-ALPS = anterior/middle/posterior diffusion along perivascular space index; g/a/m/pBOLD-CSF coupling = the coupling between blood-oxygen-level-dependent signals from global/anterior/middle/posterior cortical gray matter and cerebrospinal fluid signals; FA = fractional anisotropy; ROIs = regions of interests; JHU atlas = Johns Hopkins University atlas.

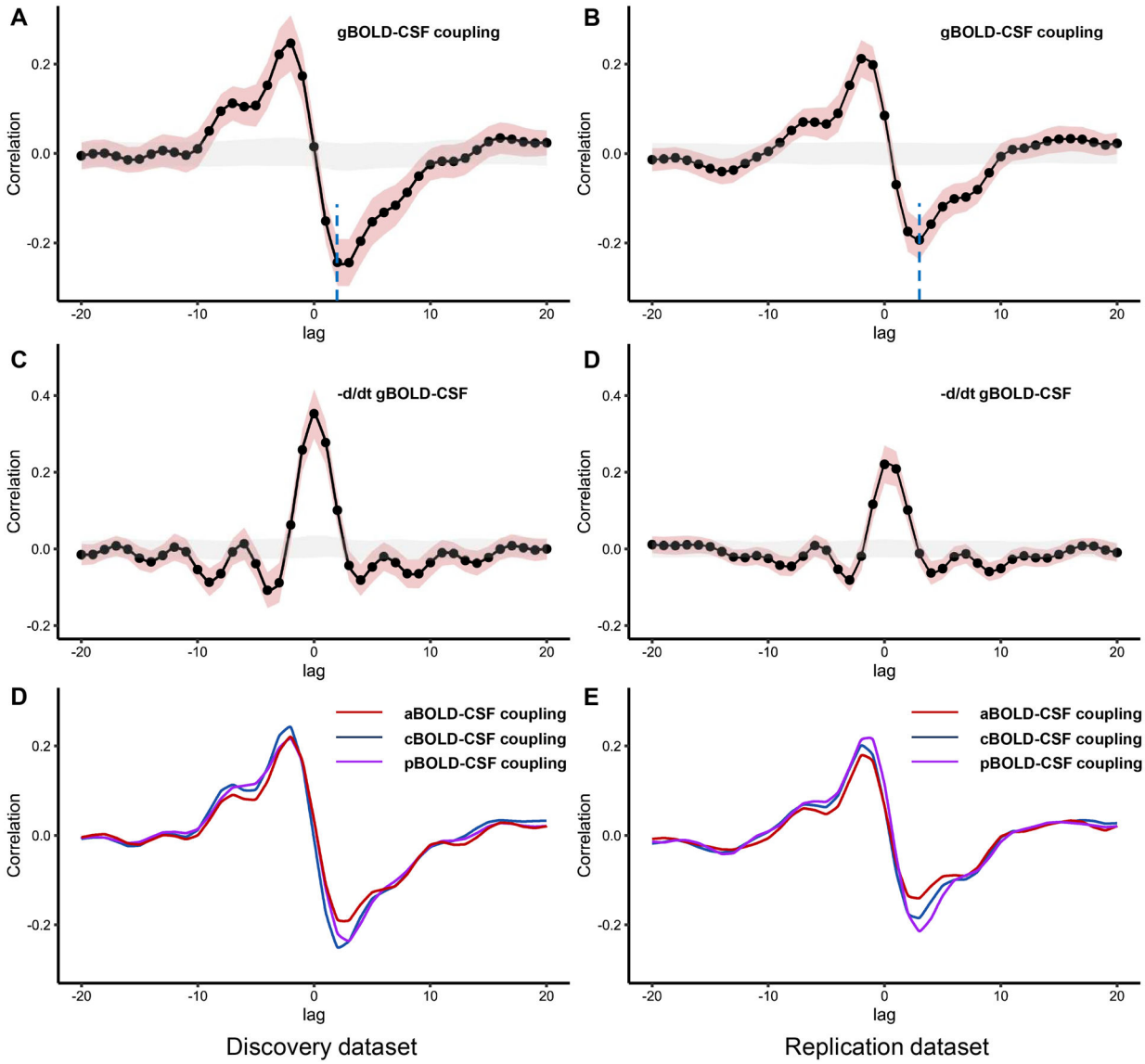

Figure 3: The cross-correlation analysis between the BOLD signal and the CSF signal.

(A-B) The mean gBOLD-CSF cross-correlation function (−20~+20s) displays positive peaks at time lags −2~−3 s (r = 0.21–0.24, $P < 0.001$, permutation test) and a negative peak at time lags 2~3 s (r = −0.19–−0.24, $P < 0.001$, permutation test; blue dotted line). **(C-D)** The mean negative first-order derivative gBOLD signals couple with CSF signals. Large positive peaks are seen at time lags 0s (r = 0.22–0.35, $P < 0.001$, permutation test). **(E-F)** Anterior, middle, and posterior BOLD-CSF coupling show different coupling strength at negative peaks. Shaded red is 95% interval of the mean correlation coefficient across subjects. Shaded grey is 95% interval of mean correlation coefficient across random pairs 1000 times repeatedly. g/a/m/pBOLD-CSF coupling = the coupling between blood-oxygen-level-dependent signals from global/anterior/middle/posterior cortical gray matter and cerebrospinal fluid signals.

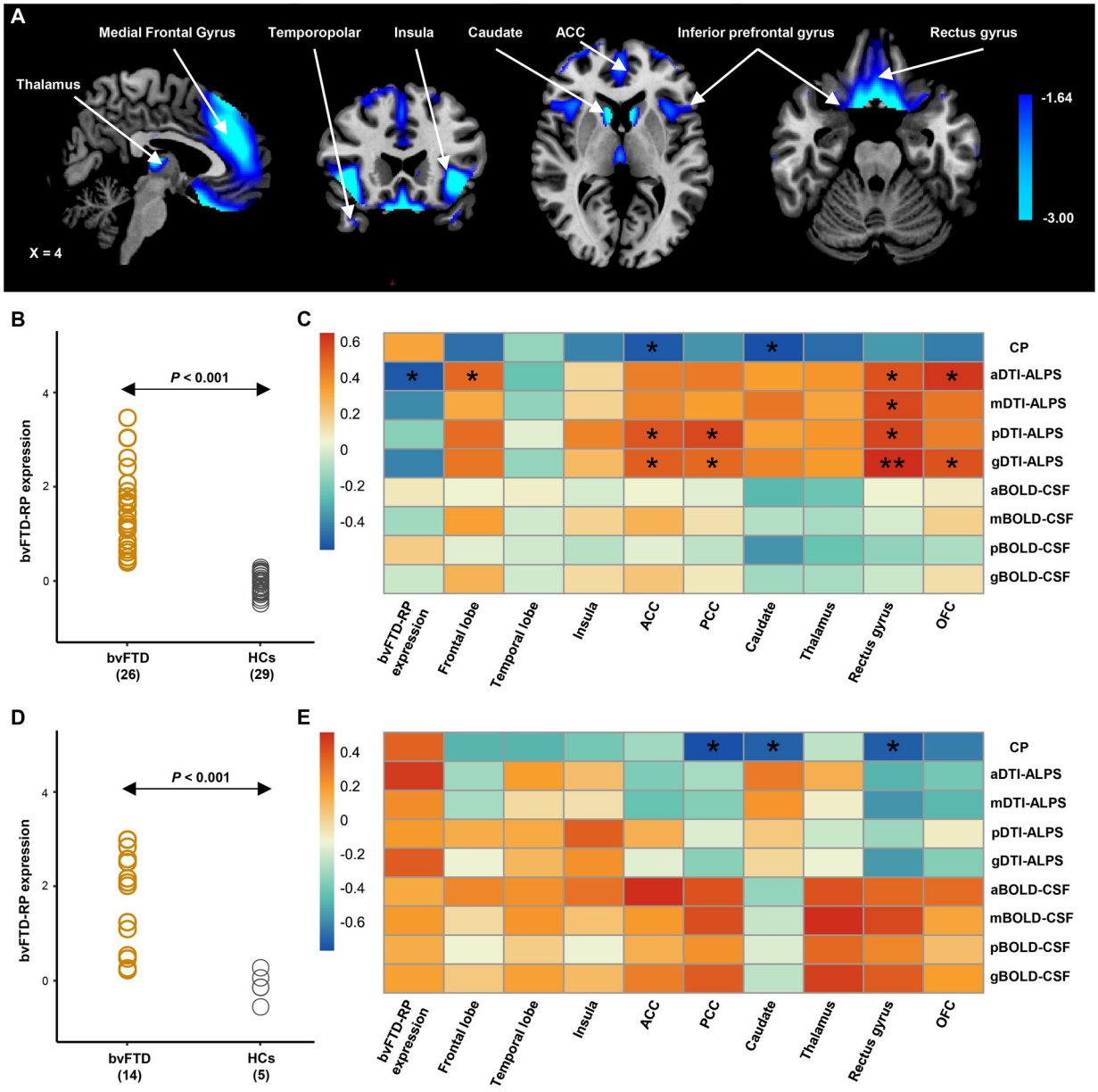

Figure 4: Behavioral variant frontotemporal dementia-related pattern (bvFTD-RP) and the spatial correlation with the glymphatic function.

(**A**) The bvFTD-RP was identified from the ^{18}F-FDG PET data of 26 patients with bvFTD and 29 age- and sex-matched healthy controls from the discovery dataset using the spatial covariance analysis (SSM/PCA). Voxel weights on metabolic network regions reliable based on bootstrap estimation. Metabolic reductions were observed in bilateral metabolic reductions in the thalamus, caudate, insular, ACC, OFC, rectus gyrus, inferior and middle frontal gyrus, and temporopolar. (**B**) Individual bvFTD-RP expression significantly ($P <$ 0.001, Student's t test between groups) separated the bvFTD patients from the healthy controls from the discovery dataset, and this finding was validated in the replication dataset **(D)**. **(C-E)** Heatmap shows the partial correlation analysis between glymphatic measures and the bvFTD-RP expression and the regional SUVRs value of nine ROIs in bvFTD patients

from the discovery dataset **(C)** and replication dataset **(E)**. *P* values were adjusted for age, sex and frontotemporal volume, and corrected for multiple comparisons using the false discovery rate approach. g/a/m/pDTI-ALPS = global/anterior/middle/posterior diffusion along perivascular space index; g/a/m/pBOLD-CSF coupling = the coupling between blood-oxygen-level-dependent signals from global/anterior/middle/posterior cortical gray matter and cerebrospinal fluid signals; SUVRs= standardized uptake value ratios; ACC = anterior cingulate gyri; PCC = posterior cingulate gyri; OFC = orbitofrontal cortex; bvFTD = behavioral variant frontotemporal dementia; HCs = healthy controls. $*P < 0.05$, $**P < 0.01$.

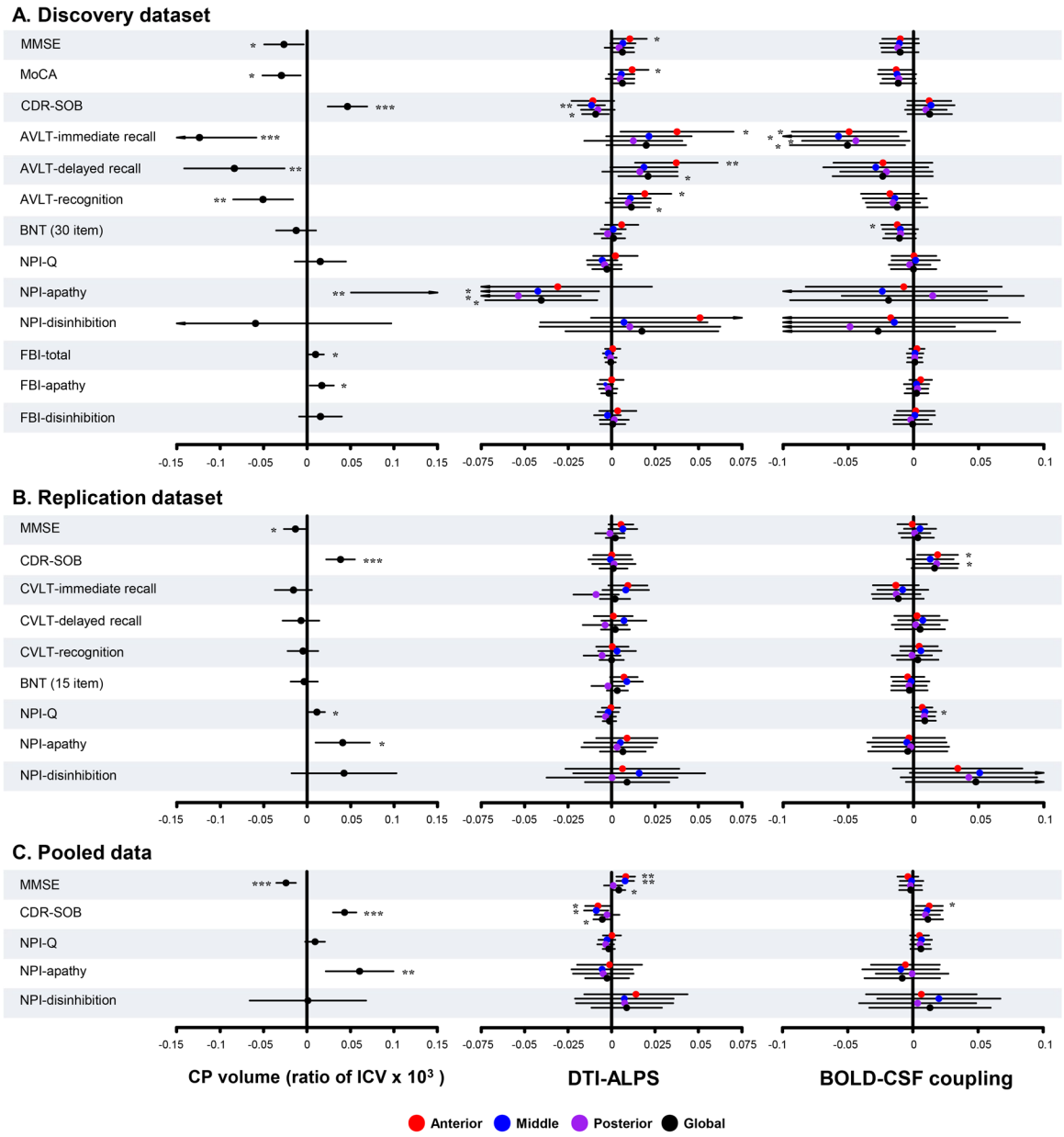

Figure 5: Regression analysis between glymphatic measures and neuropsychological test scores.

Forest plots show the results in the discovery dataset (**A**), the replication dataset (**B**), and the pooled data (**C**). The X axis shows the unstandardized β. *P* values were adjusted for age, sex, years of education, frontotemporal volume (discovery dataset), and scanning sites (replication dataset and pooled data). MMSE = Mini-Mental State Examination; MoCA = Montreal Cognitive Assessment; BNT = Boston Naming Test; AVLT = Auditory verbal learning test; CVLT = California Verbal Learning Test; CDR = Clinical Dementia Rating score; SOB = sum of boxes; NPI-Q = Neuropsychiatry Inventory Questionnaire; FBI = Frontal Behavioral Inventory; CP = choroid plexus; ICV = intracranial volume; g/a/m/pDTI-ALPS = global/anterior/middle/posterior diffusion along perivascular space index; g/a/m/pBOLD-CSF coupling = the coupling between blood-oxygen-level-dependent signals from

global/anterior/middle/posterior cortical gray matter and cerebrospinal fluid signals. *P < 0.05, **P < 0.01, ***P < 0.001.

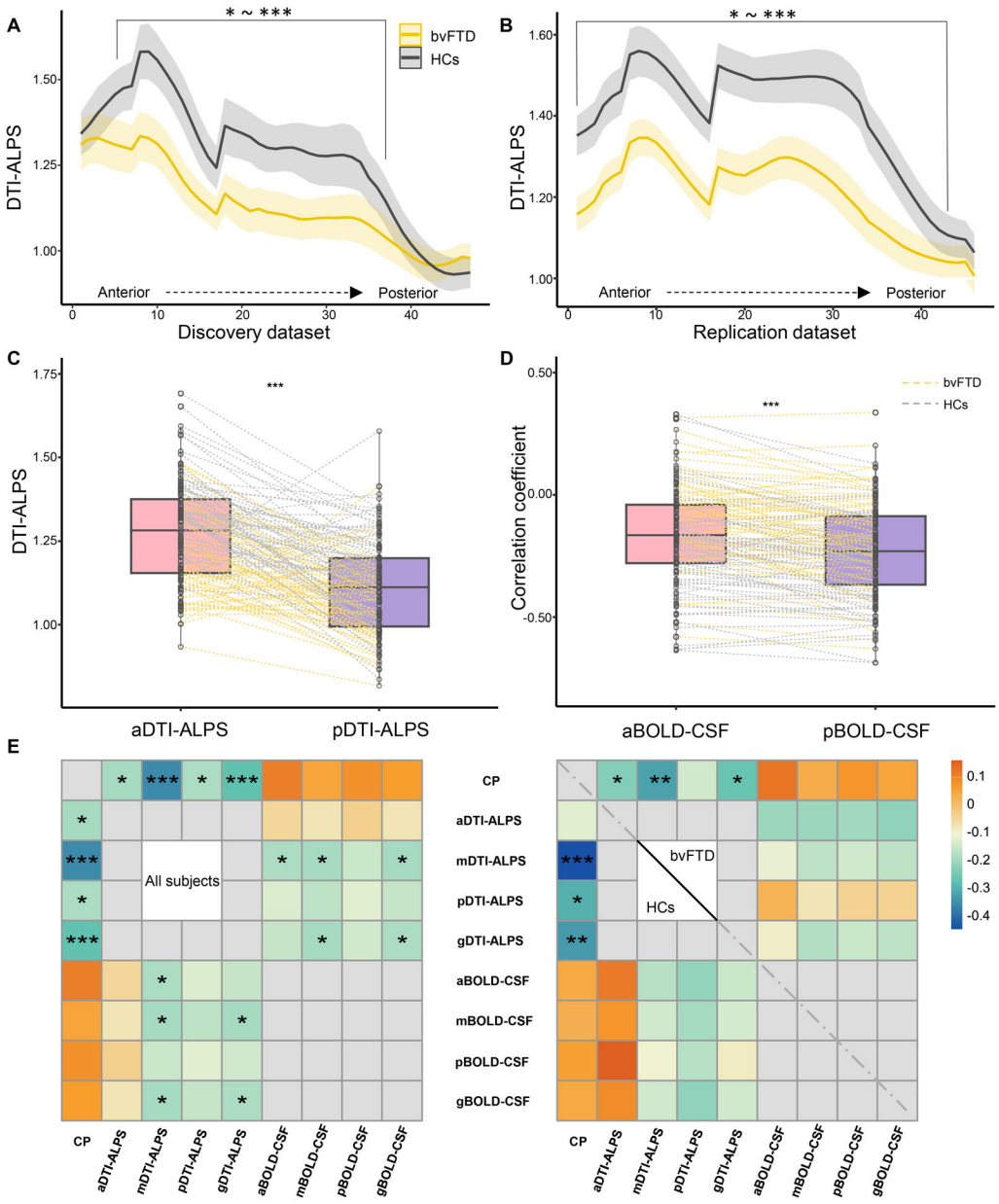

Figure 6: Glymphatic gradient and the relationship between different regional glymphatic functions.

(A-B) show the DTI-ALPS gradient and inter-group differences. **(C-D)** show the paired-sample t-test between aDTI-ALPS and pDTI-ALPS, and aBOLD-CSF coupling and pBOLD-CSF coupling, respectively. **(E)** Heatmaps show the relationship between glymphatic measures in the whole cohort and in the groups separately. *P* values in heatmaps were adjusted for age, sex, scanning sites (right), and groups (left). bvFTD = behavioral variant frontotemporal dementia; HCs = healthy controls. CP = choroid plexus; ICV = intracranial volume; g/a/m/pDTI-ALPS = global/anterior/middle/posterior diffusion along perivascular space index; g/a/m/pBOLD-CSF coupling = the coupling between blood-

oxygen-level-dependent signals from global/anterior/middle/posterior cortical gray matter and cerebrospinal fluid signals. *$P < 0.05$, **$P < 0.01$, ***$P < 0.001$.

Table1

Demographic and neuropsychiatric assessment of patients with bvFTD and health controls (HCs).

	Discovery dataset			Replication dataset[c]			bvFTD[d]	HCs[d]
	bvFTD (N=26)	HCs (N=29)	*P* value	bvFTD (N=48)	HCs (N=38)	*P* value	*P* value	*P* value
Mean age, y	63.00 (7.73)	60.31 (8.31)	0.221	60.72 (5.97)	60.03 (7.15)	0.792	0.164	0.881
Gender, male	10 (38.46%)	11 (37.93%)	0.968	33 (64.58%)	17 (44.74%)	0.104	**0.031**	0.576
Education, y	10.04 (4.75)	10.38 (3.91)	0.771	15.58 (3.03)	16.50 (2.10)	0.53	**<0.001**	**<0.001**
ICV (ml)	1447.69 (152.38)	1423.52 (103.83)	0.900	1551.02 (159.66)	1475.12 (166.44)	0.051	**0.009**	0.361
Cortex (ml)	401.33 (51.39)	459.69 (33.39)	**<0.001**	395.85 (56.72)	443.19 (40.61)	**<0.001**	0.684	**0.036**
WML (ml)	8.16 (6.73)	3.73 (10.15)	**<0.001**	13.83 (16.68)	1.70 (3.39)	**<0.001**	0.698	0.158
MMSE	17.65 (6.03)	28.66 (1.88)	**<0.001**	24.79 (4.31)	29.26 (0.86)	**<0.001**	**<0.001**	0.345
MoCA	11.28 (6.02)	25.17 (2.53)	**<0.001**	-	-	-	-	-
BNT (30[a]/15[b]item)	20.04 (6.88)	28.31 (2.07)	**<0.001**	12.01 (3.71)	14.55 (0.80)	**<0.001**	-	-
AVLT[a]/CVLT[b]-immediate recall	3.12 (1.93)	7.84 (1.88)	**<0.001**	4.27 (2.84)	8.03 (1.20)	**<0.001**	-	-
AVLT[a]/CVLT[b]-delayed recall	1.73 (2.55)	8.41 (2.91)	**<0.001**	3.35 (3.07)	7.63 (1.36)	**<0.001**	-	-
AVLT[a]/CVLT[b]-recognition	2.24 (3.90)	11.55 (2.46)	**<0.001**	6.42 (3.34)	8.21 (2.08)	**0.009**	-	-
CDR-SOB	7.90 (4.68)	-	-	5.86 (3.12)	-	-	0.098	-
NPI-Q	5.96 (4.89)	-	-	12.77 (6.37)	-	-	**<0.001**	-
NPI-apathy severity	1.73 (1.12)	-	-	1.94 (1.80)	-	-	0.176	-
NPI-disinhibition severity	0.5 (0.99)	-	-	1.50 (1.11)	-	-	**<0.001**	-
FBI-total	21.85 (14.12)	-	-	-	-	-	-	-
FBI-apathy	15.65 (9.39)	-	-	-	-	-	-	-
FBI-disinhibition	6.19 (5.95)	-	-	-	-	-	-	-

Data are presented as mean ± SD or n (%). bvFTD = behavioral variant frontotemporal dementia; HCs = healthy controls; SD = standard deviation; ICV = intracranial volume; MMSE = Mini-Mental State Examination; MoCA = Montreal Cognitive Assessment; BNT = Boston Naming Test; AVLT = Auditory verbal learning test; CVLT = California Verbal Learning Test; CDR = Clinical Dementia Rating score; SOB = sum of boxes; NPI-Q = Neuropsychiatry Inventory Questionnaire; FBI = Frontal Behavioral Inventory.

[a] In discovery dataset;

[b] in replication dataset;

[c] *P*-values were adjusted for scanning sites;

[d] Discovery dataset versus replication dataset.

Table 2

Between-group comparison of CP, DTI-ALPS, and BOLD-CSF coupling

	Discovery dataset			Replication dataset[c]			bvFTD[d]	HCs[d]
	bvFTD (N=26)	**HCs (N=29)**	***P* value**	**bvFTD (N=48)**	**HCs (N=38)**	***P* value**	***P* value**	***P* value**
CP volume								
CP (ml)	1.96 (0.58)	1.22 (0.31)	**<0.001/<0.001** [a]	1.86 (0.36)	1.16 (0.33)	**<0.001/<0.001** [a]	0.412	0.421
CP (ratio of ICV × 10^3)	1.35 (0.36)	0.85 (0.20)	**<0.001/<0.001** [a]	1.20 (0.21)	0.78 (0.19)	**<0.001/<0.001** [a]	**0.033**	0.159
DTI-ALPS								
aDTI-ALPS	1.25 (0.16)	1.37 (0.12)	**0.002/0.015**[a]/ 0.494[b]	1.17 (0.10)	1.34 (0.12)	**<0.001/<0.001** [a] / **<0.001** [b]	**0.019**	0.277
mDTI-ALPS	1.12 (0.11)	1.27 (0.15)	**<0.001/<0.001**[a]/ 0.174[b]	1.21 (0.11)	1.40 (0.14)	**<0.001/<0.001** [a] / **<0.002** [b]	**0.002**	**<0.001**
pDTI-ALPS	1.04 (0.11)	1.09 (0.13)	0.134/0.245[a]/ 0.639[b]	1.08 (0.12)	1.21 (0.14)	**<0.001/<0.001**[a]/ **0.004**[b]	0.098	**<0.001**
gDTI-ALPS	1.14 (0.10)	1.24 (0.11)	**0.001/0.006**[a]/ 0.509[b]	1.16 (0.07)	1.31 (0.10)	**<0.001/<0.001**[a]/ **<0.001**[b]	0.353	**0.008**
BOLD-CSF coupling								
aBOLD-CSF	−0.14 (0.20)	−0.27 (0.22)	**0.009/0.045** [a]	−0.08 (0.17)	−0.23 (0.19)	**0.001/0.016** [a]	0.332	0.382
mBOLD-CSF	−0.20 (0.21)	−0.32 (0.20)	**0.028**/0.060[a]	−0.13 (0.18)	−0.27 (0.19)	**0.003**/0.054[a]	0.157	0.277
pBOLD-CSF	−0.17 (0.19)	−0.32 (0.18)	**0.004/0.010** [a]	−0.17 (0.18)	−0.29 (0.19)	**0.014**/0.148[a]	0.996	0.532
gBOLD-CSF	−0.19 (0.20)	−0.31 (0.20)	**0.029**/0.064[a]	−0.14 (0.18)	−0.28 (0.19)	**0.003/0.047** [a]	0.264	0.524

Data are presented as mean (SD). bvFTD = behavioral variant frontotemporal dementia; HCs = healthy controls; CP = choroid plexus; ICV = intracranial volume; g/a/m/pDTI-ALPS = global/anterior/middle/posterior diffusion along perivascular space index; g/a/m/pBOLD-CSF coupling = the coupling between blood-oxygen-level-dependent signals from global/anterior/middle/posterior cortical gray matter and cerebrospinal fluid signals.

[a] Cortical gray matter volume-adjusted *P* value;

[b] Cortical gray matter volume-, white matter lesion volume- and intracranial volume-adjusted *P* value;

[c] *P*-values were adjusted for scanning sites;

[d] Discovery dataset versus replication dataset.